Experimental passive and reactive control of a laboratory scale WEC point absorber

Bret Bosma, Courtney Beringer, Bryson Robertson

Abstract—**Laboratory scaled testing of wave energy converters is a valuable step in the development of a WEC concept as well as a targeted application focused research effort. This paper details a portion of the initial experimental test campaign of the open-source Laboratory Upgrade Point Absorber (LUPA) WEC. A description of the LUPA device and details of the power take off system are followed by experimental results, numerical modelling comparison, and suggestions for future work. Experimental testing at the O.H. Hinsdale Wave Research Laboratory at Oregon State University is detailed as well as numerical modelling using WEC-Sim. Two basic control strategies are explored, namely velocity proportional, and velocity and position proportional feedback control, also called passive and reactive control. Results are summarized for maximum average power and capture width showing a potential for greater average energy production using reactive feedback control. A capture width increase of three times was realized as compared to passive feedback for certain cases. Numerical results from WEC-Sim are compared to experimental results showing a good average power match for passive feedback and relatively low damping values. LUPA provides an open-source experimental model of a generic wave energy converter useful for WEC research.**

Keywords—**laboratory testing, point absorber, scaled prototype, WEC control**

This paper is based upon work supported by the United States Department of Energy under Award Number DE-EE0008955. Neither the United States Government nor any agency thereof, nor any of their employees, makes any warranty, expressed or implied, or assumes any legal liability or responsibility for the accuracy, completeness, or usefulness of any information, apparatus, product, or process disclosed, or represents that its use would not infringe upon privately owned rights. Reference herein to any specific commercial product, process, or service by trade name, trademark, manufacturer, or otherwise does not necessarily constitute or imply its endorsement, recommendation, or favoring by the United States Government or any agency thereof. The views and opinions of the authors expressed herein do not necessarily state or reflect those of the United States Government or any agency thereof.

B. Bosma is with the O. H. Hinsdale Wave Research Laboratory, Oregon State University Corvallis, OR 97331 U.S.A (e-mail: bret.bosma@oregonstate.edu).

C. Beringer is with the Pacific Marine Energy Center (PMEC), Oregon State University, Corvallis, OR 97331 U.S.A. (email: beringec@oregonstate.edu).

B. Robertson is with the Pacific Marine Energy Center (PMEC), Oregon State University, Corvallis, OR 97331 U.S.A. (email: bryson.robertson@oregonstate.edu).

Digital Object Identifier: https://doi.org/10.36688/ewtec-2023-184

I. Introduction

OCEAN wave energy converter research continues to be a rich area of study as alternatives to fossil fuel energy generation are pursued in light of climate change as a result of greenhouse gas emissions. Countless concepts and designs of WECs have been conceived with many progressing through technology readiness levels and technology performance levels [1]. A key early-stage development step is the experimental testing of a scaled prototype WEC concept. Scaled testing can verify and validate numerical models, get a first glimpse at conversion efficiency and practical limitations, and expose challenges that are more difficult to realize through numerical models. Furthermore, scaled models can be a test bed for control algorithms used to maximize energy capture, test out mooring schemes, and study hydrodynamic properties.

WEC control has been a popular area of research as the advantages of a properly designed and controllable system are immense. Adaptive [2] and optimum [3] control techniques show promise in maximizing energy capture. However, most of this research has been done numerically, with limited experimental verification and validation realized at small or full scale.

This paper details experimental testing of the LUPA WEC [4], a laboratory scale WEC, to establish baseline power capture results for velocity proportional damping feedback control. It also explores the addition of position proportional stiffness feedback control term and its potential benefits and drawbacks. A numerical model of the LUPA is also developed, and results compared with the experimental velocity proportional damping only case.

The LUPA device consists of two bodies, namely a float and a spar. The float sits at the water surface and is excited by the change in wave surface elevation and related pressures. The hull shape is a cylinder with a large chamfer underwater. Motivation for this shape is given in [5] as it provides maximum absorbed power compared to other simple shapes investigated. The spar

is a slender body that rises through the centre of the float and has a large heave plate at the bottom. This heave plate is designed to resist heave motion, through significant added mass, and is located at the bottom where the influence of the incident wave is minimal. The relative motion between the active float and stationary spar provides an opportunity for energy harvest. The so-called Power Take Off (PTO) system converts this relative motion into useful energy.

II. PTO PASSIVE AND REACTIVE CONTROL

In building a scaled prototype of a WEC, the PTO is the essential component if emulation of power extraction is to be realized. The PTO takes the hydrodynamic energy from the waves and transfers that energy to another form. For most realizations the goal of the WEC is electrical energy. Often PTOs include a change in fluid, such as oscillating water column use of pneumatic, or point absorbers with a hydraulic PTO system. These change in fluids inherently have associated losses and thus direct drive PTO solutions have generally been thought to have an advantage over systems that change fluids [6].

In this paper, the LUPA heaving point absorber is considered as shown under test in Fig. 1. The oscillatory nature of this type of device operating in typical wave conditions sets up a scenario of relatively high forces and low speeds. Assuming that we are interested in electrical energy as our output, a rotary motor/generator has a particular appeal. At first glance a linear motor/generator might seem a good choice as the mechanical conversion would be minimized. However, upon closer investigation, the cost efficiency of linear machines is lower than rotary machines because of the lack of constant interaction of entire magnet and coil, requiring a more expensive system for the same energy rating [6]. Thus, rotary machines are often used with a linear to rotary mechanical conversion employed.

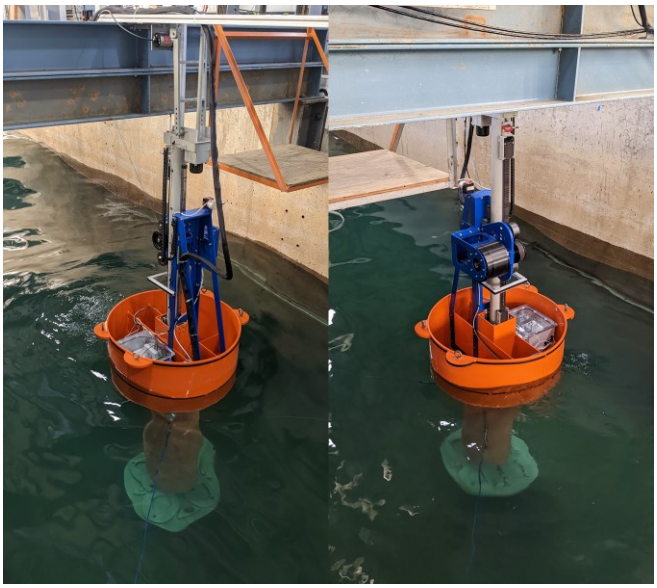

Fig. 1. LUPA device shown under test at the O.H. Hinsdale Wave Research Laboratory at Oregon State University. LUPA is a heaving two body point absorber designed to work in three modes. One body heave only, two body heave only, and two body six degrees of freedom. Images above show the one body heave only mode analysed in this paper.

A. *Passive control*

Passive control is defined here as the PTOs ability to *only* absorb energy from the waves. This is typically done with one of two methods at laboratory scale. Perhaps the simplest is the use of a dashpot, or mechanical damper, which is a device that resists motion via viscous friction. The resulting force is proportional to velocity and acts in opposition to the motion. They can dampen rotary or linear motion. Drawbacks to using mechanical dampers include a nonlinear response and difficulty in setting/monitoring exact damping values. Dashpots either come with a fixed damping, or a variable one that often proves challenging to set accurately.

The second method is the use of a motor/generator and associated drive applying velocity proportional damping. This works best with the implementation of a high-resolution encoder providing velocity feedback. A simple control is implemented where the velocity of the motor/generator is read and multiplied by a damping value resulting in a torque to be applied to the motor/generator in opposition to the measured motion.

It is important to consider the reference frame and units of the applied damping, especially if the goal is to compare to numerical simulation. It is likely that initial numerical modelling would not include the details of the linear to rotary conversion, thus damping would be in the

Fig. 2. Deployed LUPA power take off system. Motor/Generator and belt drive rotary to linear conversion including idler pulleys and drive sprocket.

linear motion frame. The LUPA PTO experimental setup is shown in Fig. 2. To input damping values in the experimental system that correspond to the numerical modelling, losses in the belt drive are assumed negligible and rotational damping is converted to linear damping through the sprocket.

$$\tau = B_l r^2 \omega \tag{1}$$

where τ is the motor/generator commanded torque in Newton-meters, B_l is the applied linear damping in Newton-meter per second and $B_l > 0$, r is the radius in meters of the sprocket used, and ω is the rotational velocity of the motor in radians per second.

Passive control, or velocity proportional damping is a relatively easy to implement control methodology with generally satisfactory results. Damping can be tuned for each wave condition input and provides a passive control that can be used as a baseline in comparison with more sophisticated control schemes.

B. *Reactive Control*

So-called reactive control is a feedback control technique extended from the passive velocity proportional feedback to include a position proportional term commonly referred to as stiffness. A motivation for this control scheme is the prospect of investing energy in the system for part of a cycle while harvesting a greater amount of energy on aggregate compared to velocity proportional damping.

A similar approach to applying this to LUPA involves commanding the torque

$$\tau = K_l r\theta + B_l r^2 \omega \tag{2}$$

where K_l is the applied stiffness in Newtons per meter and θ is the rotational position in radians.

III. EXPERIMENTAL SETUP

All experimental work was done at the O.H. Hinsdale Wave Research Laboratory (HWRL) at Oregon State University, USA. Tests were conducted in the Large Wave Flume (LWF) facility which is 3.7 m wide and 104 m long. The water depth was set to 2.74 m. The LUPA model was placed 29 m from the wavemaker. A 1:12 sloped beach was located onshore of the model.

Four resistance type wave gauges were located along the tank wall. Two before the model and two after located 21.28 m, 24.94 m, 32.43 m, 35.89 m from the wavemaker and 1.39 m from the centre of the tank.

The LUPA point absorber WEC is the test article, and all results in this paper are from the one body heave only configuration [4]. In this mode, the spar body is fixed, and the float body is free to move in heave only.

The PTO system consists of an Akribis ADR220-B175 motor/generator with a Renishaw Resolute BiSS-C 26-bit encoder built in. The motor/generator has 12 pole pairs with a continuous torque rating of 46 Nm. The motor drive paired is the Elmo Motion Control Gold Oboe in the 13 A / 230 V configuration. A three phase 208 V, 30 A supply was connected to the drive. The drive is EtherCAT enabled, and all control is done via the EtherCAT communications protocol. A standard USB communication is used to configure the drive using the EASII software.

There are two data acquisition systems recording data for this project. Synchronizations signals, one generated by the wavemaker, and one by a random delay square wave module are recorded on both acquisition systems. The random delay square wave generates a unique time sequence that can be cross correlated between acquisition systems to align datasets.

The HWRL operates a National Instruments PXI based acquisition system with PXI-6259 M-Series analog inputs. These modules record wave gauge data, HWRL deployed mooring load cell data, and string pot data.

The second data acquisition system is a Speedgoat performance real time machine and acts as the primary EtherCAT node with the motor/generator drive and two Beckhoff EK1100 modules acting as secondary EtherCAT nodes. One EK1100 is on the shore and has an EL3104 analog input module. This records the synchronization signals. The shoreside LUPA electrical/electronics is shown in Fig. 3 with the upper image showing the operational state and the lower showing the contents.

The second EK1100 is located on the LUPA device and records signals from the load cells on the belt, motor temperature, a draw wire measuring relative motion between spar and float, and a vertical reference unit measuring angles and velocities of the float body. These

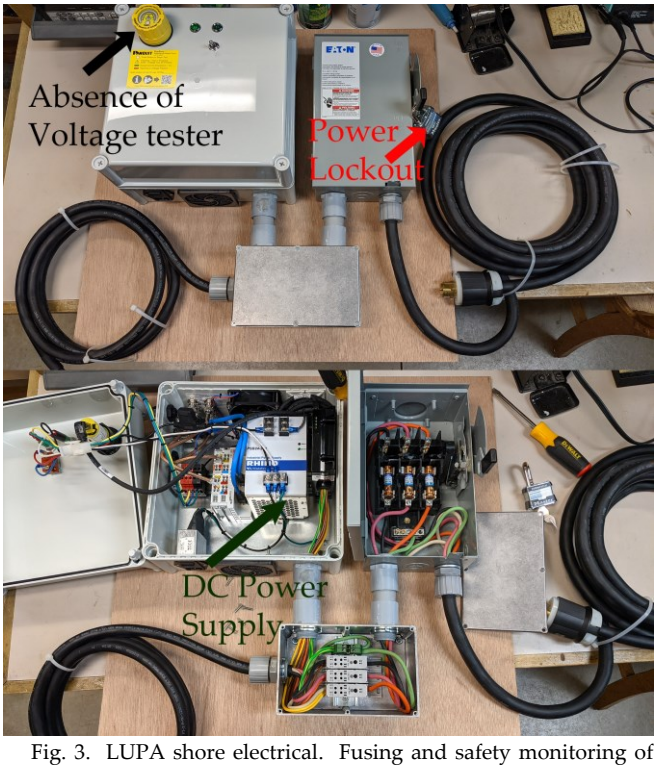

Fig. 3. LUPA shore electrical. Fusing and safety monitoring of 208 V three phase 30 A supply. Capture of data acquisition synchronization signals.

signals are captured with an associated Beckhoff module connected to the EK1100. Onboard LUPA electrical/electronics are shown in Fig. 4. A DC/DC power supply is used to create a stable 24 V electronics supply onboard to power the low power on the drive and the data acquisition instruments.

The wave conditions are all regular waves with a consistent wave height command and a sweep of periods. Two sets of data were collected, one with varying velocity proportional damping, and one with varying velocity proportional damping and position proportional stiffness as shown in Table I. The wave height was reduced for the damping and stiffness case to prevent overtopping with greater amplitude heave motion.

TABLE I
TEST CONDITIONS ANALYSED IN THIS PAPER

	T (s)
Damping	1.5, 1.75, 2, 2.25, 2.5, 2.75, 3, 3.25, 3.5
H=0.2 m	Range of Damping [0 7000] N/m/s
Damping &	1.5, 1.75, 2, 2.25, 2.5, 2.75, 3, 3.25
Stiffness	Range of Damping [0 7000] N/m/s
H=0.15 m	Range of Stiffness [-4000 7000] N/m

Waves were run on the wavemaker with linear wave theory and active wave absorption turned on. Each run consisted of time allowing for ramp up and ramp down and 20 waves for each damping value. For the damping only cases 40 damping values were run. For damping and stiffness cases 80 damping and stiffness values were run.

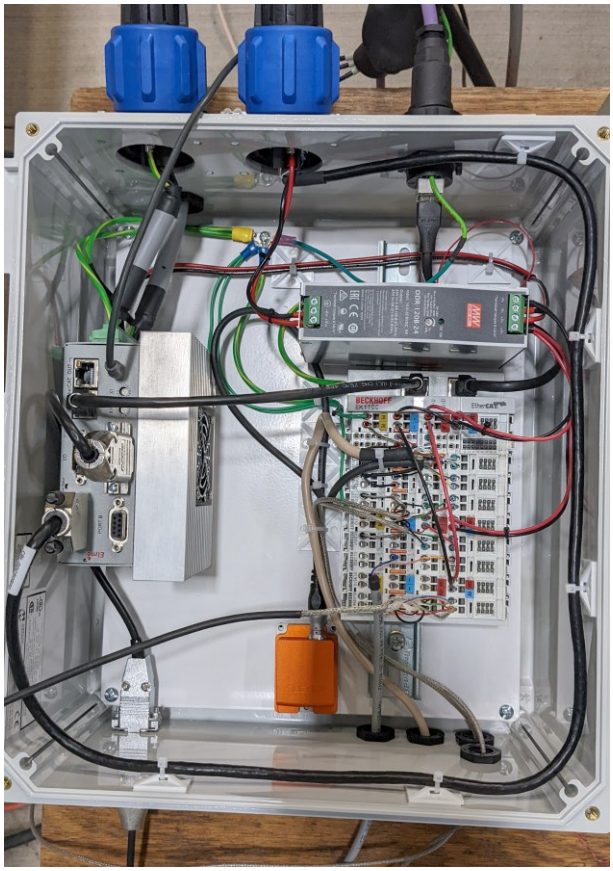

Fig. 4. Onboard LUPA electronics in water resistant box. All signals recorded on the LUPA device are captured in this box and sent over the EtherCAT network to the primary node.

For selecting the damping and stiffness values, the Latin Hypercube Sampling (LHS) technique was used [8]. LHS is a statistical method for generating a near-random sample of values. It ensures coverage of a space while keeping a random element. A range of damping values from 0 to 7000 $\frac{N}{\frac{m}{s}}$ was applied for the damping only and the damping and stiffness cases. The range of stiffness values applied to the damping and stiffness cases was -4000 to 7000 $\frac{N}{m}$.

IV. NUMERICAL MODELLING

A key tool in WEC development is having a numerical model of the device that adequately represents the physical system. Numerical models can provide valuable information about the operation of a system such as position, velocity, force, torque, and power estimates. Determining these experimentally can be costly even at small scales. Additionally, they can help with the design of the physical device and mooring systems. There are many approaches to numerical modelling of wave energy converters with a review provided here [9]. The following is the general workflow used in the numerical modelling process undertaken for this paper.

First, an as-built simplified geometry was modelled in Solidworks [10]. General dimensions were measured from the LUPA test article, and a simplified geometry of each body was created as shown in Table II. This simplified geometry was cut at the still water line and everything above the water surface was removed. The origin of the models was located at the centre of mass of the body. This was exported in the STEP file format.

Next, the STEP file was imported into Rhino3D [11]. In

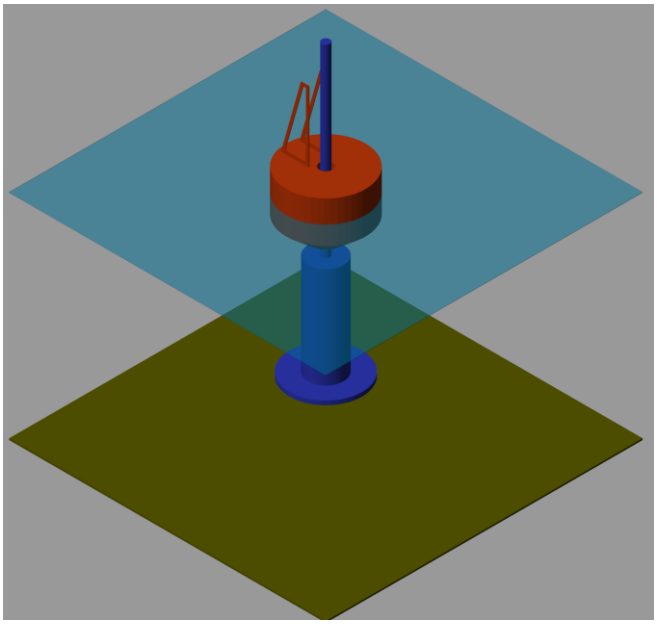

Fig. 5. WEC-Sim numerical model rendering of LUPA. Numerical model was run with experimental data for the wave elevation input and applied damping.

TABLE II
DEVICE SPECIFICATIONS

Parameter	Value	Unit
Float mass	248.72	kg
Float diameter	1.0	m
Float draft	0.44	m
Spar mass	175.54	kg
Spar heave plate diameter	0.90	m
Spar draft	2.05	m
PTO stroke length	0.5	m

the interest of computing efficiency, the simplified model is considered symmetric in both x and y, below the water surface, and the model is sliced in Rhino3D to create a quarter section. The function QuadRemesh is then used to create a mesh of the remaining geometry. This is then export in GDF format which is the mesh definition format used by WAMIT.

After running WAMIT, the output files are read by the BEMIO software which is a part of the WEC-Sim package. BEMIO takes the WAMIT output, calculates the impulse response functions, and re-formats the data into an H5 format which WEC-Sim can read.

WEC-Sim [12], a time-domain MATLAB/Simulink model based on the Cummins equation [13] was used. This modelling tool provides a good balance between speed and accuracy and is widely used in the industry and a visual of the WEC-Sim geometry is shown in Fig. 5. The WEC-Sim model is set up with the spar body fixed to the global reference frame and the Translational PTO Actuation Force block connected between the two bodies. This restricts the float body to heave only and fixes the spar body, which matches the experimental setup.

WEC-Sim wave input data was taken from the experimental testing. As discussed in section III, data from four wave gauges was collected. The data from each individual gauge was shifted from its cross-shore location to the cross-shore location of the WEC. This occurs in the frequency domain using linear wave theory. The resulting four time series are then averaged, and the result is used as the input to the WEC-Sim model. This is shown in Fig. 6 with the top four plots showing the original captured wave gauge data and the shifted version. The bottom plot shows the shifted versions together with the average of the four which is what is used as the input wave surface elevation.

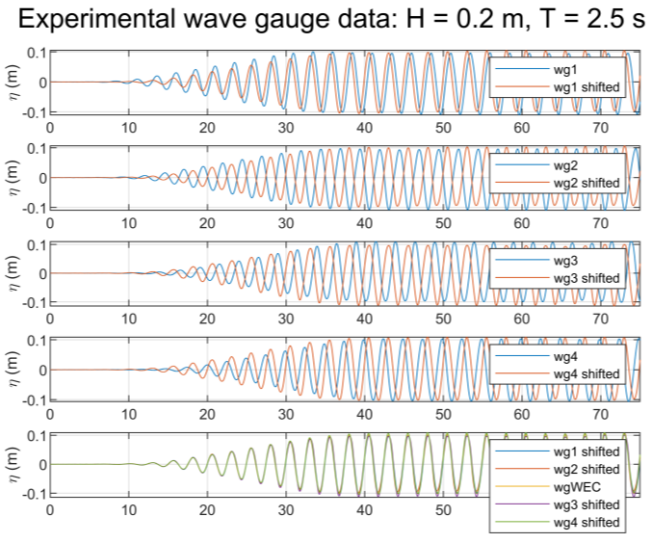

Fig. 6. Top four plots show recorded wave gauge data and the shifted version of each. The bottom plot shows the four shifted versions and the average which was used as the wave surface input for the WEC-Sim simulations.

Idealized control was implemented in the WEC-Sim Simulink model using the Translational PTO Actuation Force block between the free to heave float body and the fixed spar body. The response port is used to get instantaneous velocity and position and instantaneous damping and stiffness values from the experiment are input using the from workspace block. The resulting force is then commanded of the Translational PTO Actuation Force block in opposition to the reported motion. While this is a good first approach to numerical modelling of the feedback system, a more detailed PTO model may be required to accurately represent the system in higher damping and negative stiffness conditions as shown in the results section. It should be mentioned that [7] found that traditional linear modelling of PTOs overpredict energy capture compared to CFD nonlinear modelling.

V. RESULTS

The results of this study help characterize LUPA by providing a baseline operating result in regular waves using a velocity proportional damping control scheme. The damping only cases were modelled in WEC-Sim, highlighting the strengths and challenges of numerical modelling. Additionally, a damping and stiffness control scheme is explored experimentally to investigate its potential benefits.

Mechanical power was calculated by taking

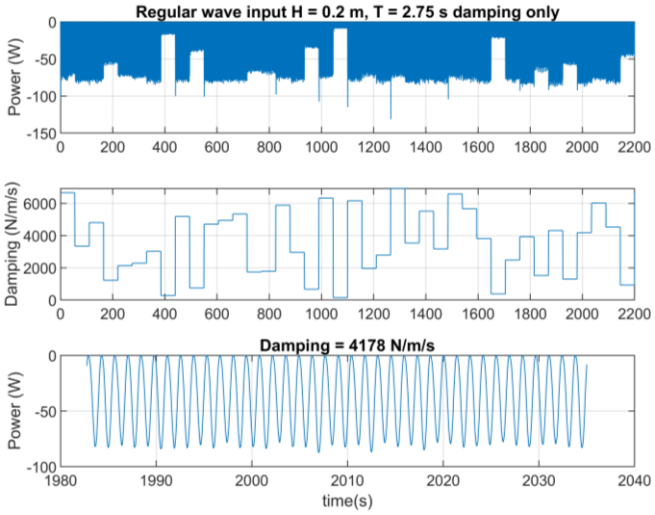

Fig. 7. Upper plot shows time series of power for varying damping values changed every twenty waves. Middle plot shows the applied damping. Lower plot shows zoomed in power time series highlighting the damping that produced maximum average power absorbed after eliminating any transition spikes.

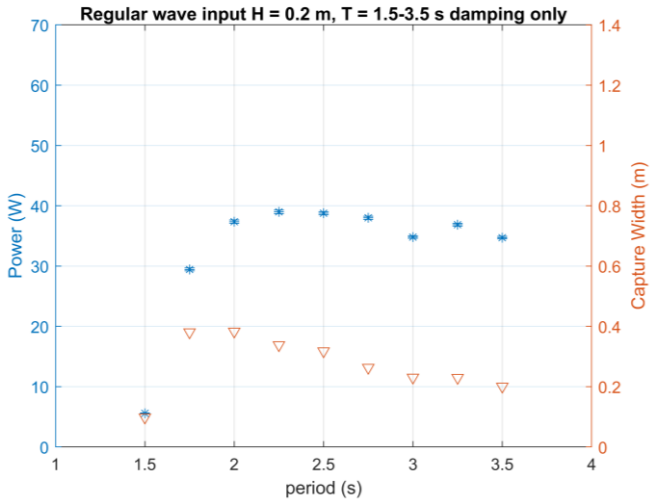

Fig. 8. Average power for damping value that provides maximum power for each period of regular wave run on left y-axis. On right y-axis the capture width for same data normalized by input wave energy flux.

instantaneous angular velocity as measured by differentiating the angular position reported by the motor/generator encoder and multiplying by the reported torque applied by the drive.

$$P = \tau\omega \tag{3}$$

The upper plot of Fig. 7 shows the time series for the absorbed mechanical power. The middle plot shows the applied damping. The bottom plot shows a zoomed in time series of the power with the applied damping that resulted in maximum average absorbed power. Notice that the convention is negative for absorbed power. Also notice that there are often spikes in power when there are steps in damping values. Because of this transient response, the first wave period after transitioning to a new damping value is removed from the average power calculations. Generally, the trend can be seen that smaller applied damping values result in smaller average power output. As damping increases, it seems that the power generally levels out.

Next, the maximum average power from each regular wave run segment is computed and plotted against input wave period as shown in the left y-axis of Fig. 8. Error bars show the uncertainty of the estimate of the power as given by two standard deviations divided by the square root of the number of samples. It is assumed that the wave height is the prescribed 0.2 m for each wave period in comparing these average power values. In practice there is variation in input wave height, so it is useful to normalize these values for comparison. Capture width provides a good metric for doing this. Capture width is defined as

$$CW = \frac{P_{avg}}{E_f} \tag{4}$$

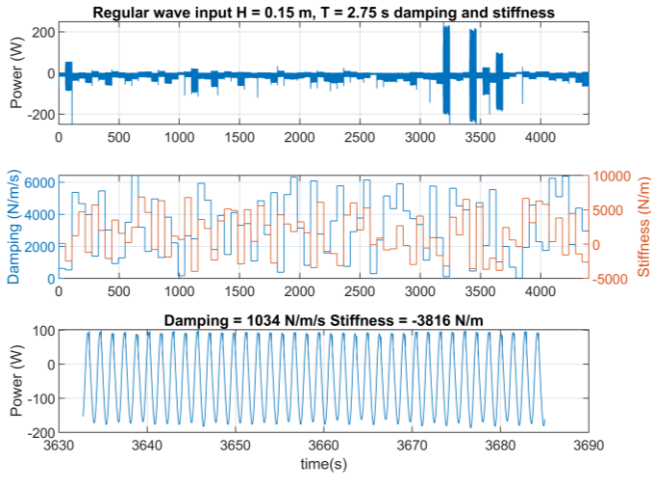

Fig. 9. Upper plot shows time series of power for varying stiffness and damping values changed every twenty waves. In the middle plot the left y-axis shows the applied damping on the right y-axis shows the applied stiffness. Lower plot shows zoomed in power time series highlighting the damping that produced maximum average power absorbed.

where P_{avg} is the average power from 19 waves for a particular damping value that provided the max average power and E_f is the energy flux

$$E_f = \frac{1}{8}\rho g H^2 c_g \tag{5}$$

where ρ is the density of water, g is the acceleration of gravity, H is the average measured wave height for the nineteen-wave segment to be analysed, and c_g is the group velocity of the wave. Notice a difference in shape between the average power and capture width results as an indication of the varying energy flux between cases.

Next, a damping and stiffness feedback term was applied to the system and a similar set of regular waves were run with a nominal wave height of 0.15 m and a sweep of periods between 1.5 and 3.25 s. Results are shown in Fig. 9 where there is both positive and negative power reported in the top plot. Positive power represents

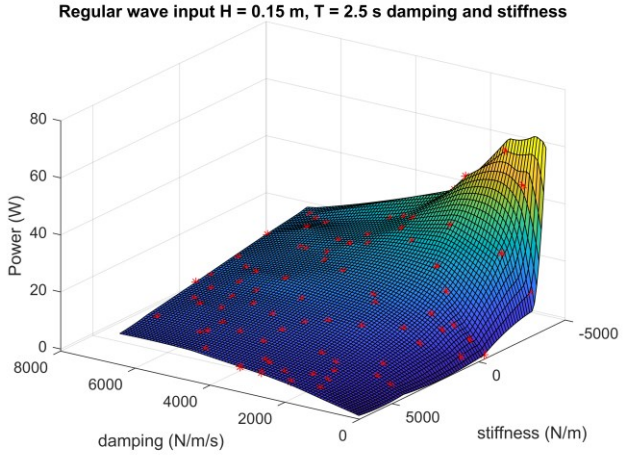

Fig. 10. Power vs. damping and stiffness for H = 0.15 m and T = 2.5 s surface plot with individual data points plotted on surface. Low damping and large negative stiffness generally produced more average power.

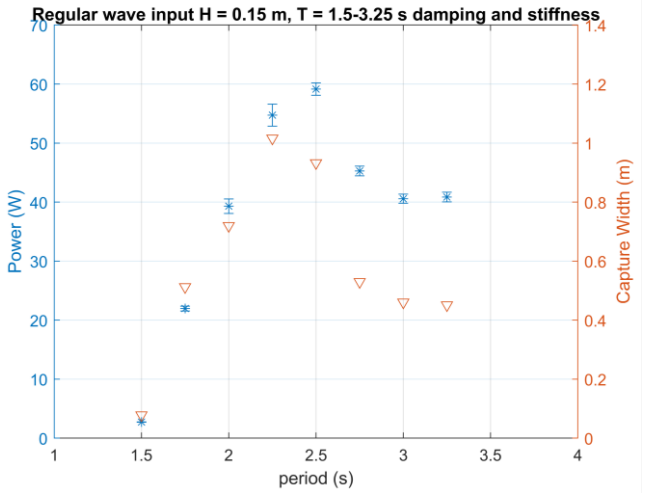

Fig. 11. Average power for the damping and stiffness value that provides maximum power for each period of regular wave run on left y-axis. On right y-axis the capture width for same data set.

power invested into the system from the drive, and negative power indicates power harvested or absorbed from the system. The goal is experimentally investigating and validating the possibility of getting more power out on average with stiffness feedback applied. The middle plot shows the applied damping on the left y-axis, and the applied stiffness on the right y-axis. The bottom plot shows a zoomed in power with an investment of almost 100 W of power peak, with a return of almost 200 W peak, and an average of about 45 W absorbed. Fig. 10 shows a power vs. damping and stiffness for the H = 0.15 m and T = 2.5 s regular wave case as a surface plot. Individual points used to create the surface are also plotted. Looking at the trends of applied damping and stiffness in the plot, a relatively low damping value and a relatively high negative stiffness value provides max average power output.

Next power vs. input wave period is shown in Fig. 11 for the damping and stiffness case. It is unfair to directly compare power results from Fig. 11 to Fig. 8 for two reasons. One, the prescribed input wave height was different (0.15 m vs. 0.2 m), and, two, the prescribed and measured wave height may vary. The normalized capture width parameter shown in the right y-axis provides a better metric to compare. At a 2.25 s period, the case with the biggest differential, the capture width from Fig. 8 to Fig. 11 increased from 0.338 m to 1.016 m, providing a three times increase for the damping and stiffness case.

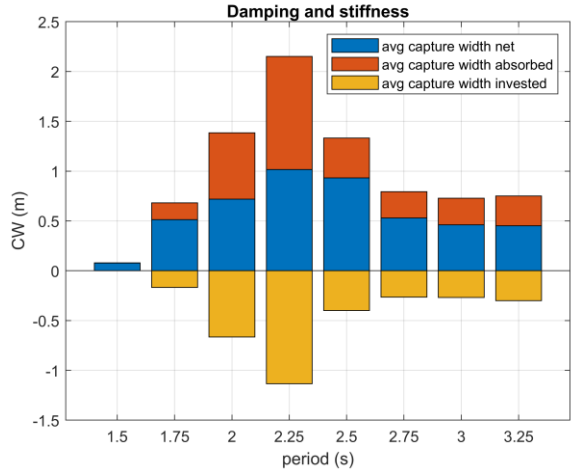

Fig. 12. Capture width vs. input wave period plot showing the contribution of invested power, absorbed power, and net power to the energy capture.

Another thing to compare in Fig. 8 and Fig. 11 is the shape of the plots. While the general trends of the plots are similar, differences in the amplitude of the input wave can skew the power results. For example, in Fig. 11, the peak power occurs at a period of 2.5 s where the peak capture width occurs at a period of 2.25 s.

The concept of investing energy in part of the generating cycle to absorb more on average is an attractive proposition likely to have ramifications for full scale PTO and energy system design. The additional forces and velocities required to achieve the additional power could mean a higher specification of equipment, for example. Higher torques and velocities could also have a negative impact on other parts of the WEC including mooring lines, seals and bearings, and PTO components. Fig. 12 shows the relative contribution of the invested and absorbed energy, from the max average power cases, on the net energy in terms of capture width. Of note is the nonlinearity. For example, at a period of 2.25 s the extra invested energy is quite high related to the net capture width gain as compared to 2.50 s.

Finally, the WEC-Sim model was used to estimate power production in regular waves. As detailed in section IV, experimentally measured wave surface elevations and applied damping and stiffness values were inputs to the model. Fig. 13 shows an average power vs. damping comparison of the experimental and numerical results for two different wave input periods. Average power is predicted very well by the numerical model for low damping values, but as the damping values increase, the results diverge. For a period of 2.75 s

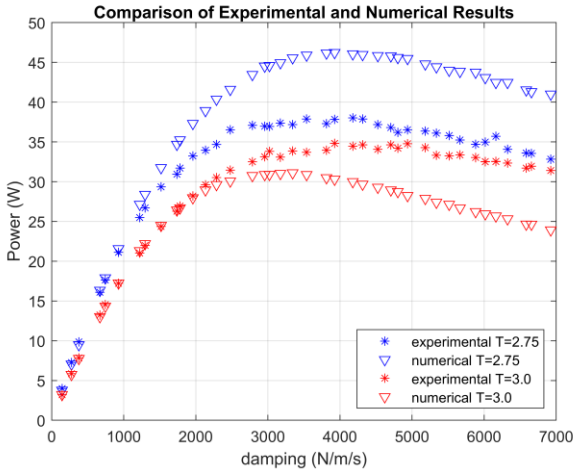

Fig. 13. Comparison of experimental and numerical results for two wave periods show the numerical model does a very good job of predicting power output for smaller damping values but can over and under predict for larger damping values depending on the input wave period.

the numerical model overpredicted, and for a period of 3.00 s the numerical model underpredicted power. This serves to highlight the nonlinearity of the power take off system and the need for a more complex PTO model at higher damping values to represent the experimental system.

Damping and stiffness feedback control numerical models were attempted, however the WEC-Sim model became unstable when negative stiffness was applied. This is likely due to the model formulation as the software tool should be able to handle this case. Future work includes improving the WEC-Sim model with a more complex PTO model capable of simulating the damping and stiffness feedback case.

VI. CONCLUSIONS

This paper serves as a documentation of the LUPA power take off system and a portion of the initial LUPA experimental test campaign and detail of a simple control scheme to provide a baseline for future work. Average power in regular waves is analysed experimentally and a stiffness feedback term was explored for using bi-directional power flow to increase average power generation. A numerical model of the system was also created, and the output was compared with experimental results for the velocity proportional damping only feedback case.

Major findings from this research include the potential for reactive control to increase the average power output of a WEC device under regular wave conditions and the parameters that optimize this condition. A capture width increase of up to three times was recorded for reactive control under certain wave conditions when compared to the optimized passive control.

Future work has a lot of potential directions as LUPA has been designed to be a test platform adaptable for many research applications. Improving the PTO model used in the WEC-Sim simulations could prove valuable in matching experimental results. Testing more advanced control schemes such as impedance matching [14] and model predictive control [15] could yield higher average power output. Structural testing on LUPA can help inform industry on materials and manufacturing implications. Uncertainty analysis on LUPA can help build confidence in experimental testing and results. LUPA provides a valuable robust test platform that can be used in many applications.

REFERENCES

[1] J. Weber, "WEC Technology Readiness and Performance Matrix–finding the best research technology development trajectory," in *Proceedings of the 4th International Conference on Ocean Energy, Dublin, Ireland*, 2012.

[2] J. Hals, J. Falnes, and T. Moan, "A Comparison of Selected Strategies for Adaptive Control of Wave Energy Converters," *J. Offshore Mech. Arct. Eng.*, vol. 133, no. 3, pp. 031101–12, 2011, doi: 10.1115/1.4002735.

[3] J. Falnes, "Optimum control of oscillation of wave-energy converters," in *The Eleventh International Offshore and Polar Engineering Conference*, OnePetro, 2001.

[4] B. Bosma, C. Beringer, and B. Robertson, "Design and modeling of a laboratory scale WEC point absorber," in *EWTEC 2021 - Plymouth, UK*, Plymouth, UK, 2021. [Online]. Available: https://proceedings.ewtec.org/product/ewtec-2021-plymouth-uk/

[5] G. Bacelli, S. J. Spencer, D. C. Patterson, and R. G. Coe, "Wave tank and bench-top control testing of a wave energy converter," *Appl. Ocean Res.*, vol. 86, no. C, Art. no. SAND2019-3344J, Mar. 2019, doi: 10.1016/j.apor.2018.09.009.

[6] M. Blanco *et al.*, "Recent Advances in Direct-Drive Power Take-Off (DDPTO) Systems for Wave Energy Converters Based on Switched Reluctance Machines (SRM)," in *Ocean Wave Energy Systems: Hydrodynamics, Power Takeoff and Control Systems*, A. Samad, S. A. Sannasiraj, V. Sundar, and P. Halder, Eds., in Ocean Engineering & Oceanography. Cham: Springer International Publishing, 2022, pp. 487–532. doi: 10.1007/978-3-030-78716-5_17.

[7] C. Windt, N. Faedo, M. Penalba, F. Dias, and J. V. Ringwood, "Reactive control of wave energy devices – the modelling paradox," *Appl. Ocean Res.*, vol. 109, p. 102574, Apr. 2021, doi: 10.1016/j.apor.2021.102574.

[8] G. D. Wyss and K. H. Jorgensen, "A user`s guide to LHS: Sandia`s Latin Hypercube Sampling Software," Sandia National Lab. (SNL-NM), Albuquerque, NM (United States), SAND-98-0210, Feb. 1998. doi: 10.2172/573301.

[9] Y. Li and Y.-H. Yu, "A synthesis of numerical methods for modeling wave energy converter-point absorbers," *Renew. Sustain. Energy Rev.*, vol. 16, no. 6, pp. 4352–4364, 2012.

[10] "3D CAD Design Software SolidWorks." http://www.solidworks.com/ (accessed Jun. 13, 2012).

[11] R. M. & Associates, "Rhinoceros 3D," *www.rhino3d.com*. https://www.rhino3d.com/ (accessed Mar. 08, 2021).

[12] "WEC-Sim (Wave Energy Converter SIMulator) — WEC-Sim documentation." https://wec-sim.github.io/WEC-Sim/ (accessed Mar. 27, 2017).

[13] W. Cummins, "The impulse response function and ship motions," *Schiffstechnik*, vol. 9, pp. 101–109, 1962.

[14] G. Bacelli, V. Nevarez, R. G. Coe, and D. G. Wilson, "Feedback Resonating Control for a Wave Energy Converter," *IEEE Trans. Ind. Appl.*, vol. 56, no. 2, Art. no. SAND-2020-0174J, Dec. 2019, doi: 10.1109/TIA.2019.2958018.

[15] T. K. A. Brekken, "On Model Predictive Control for a point absorber Wave Energy Converter," in *PowerTech, 2011 IEEE Trondheim*, Jun. 2011, pp. 1–8. doi: 10.1109/PTC.2011.6019367.